ACS OMEGA

http://pubs.acs.org/journal/acsodf

Article

Band Structure Engineering and Optical Properties of Pristine and Doped Monoclinic Zirconia (m-ZrO_2): Density Functional Theory Theoretical Prospective

El-Sayed R. Khattab,* Sayed S. Abd El Rehim, Walid M. I. Hassan, and Tamer S. El-Shazly

Cite This: *ACS Omega* 2021, 6, 30061−30068

Read Online

ACCESS | Metrics & More | Article Recommendations | Supporting Information

ABSTRACT: Recently, monoclinic ZrO_2 has received great technological importance because of its remarkable dielectric properties, high chemical stability, and high melting point. Herein, we introduce first-principles calculations using the Hubbard approach (DFT + U) to study the effects of doping with Nb and W on the electronic and optical properties of pristine ZrO_2. The introduction of dopant atoms into the pristine crystal structure led to the displacement of the bandgap edges and reallocation of the Fermi level. The valence band maximum (VBM) shifted upward, resulting in band gap tightening from 5.79 to 0.89 for ZrO_2: Nb and to 1.33 eV for ZrO_2: W. The optical absorption of doped crystals extended into the visible and near-infrared regions. Partial density of states (PDOS) calculations showed valence band dependency on the O 2p orbital energy, with the conduction band predominantly composed of Nb 4d and W 5d. For pristine ZrO_2, the results obtained for the imaginary and real parts of the dielectric function, the refractive index, and the reflectivity show good agreement with the available experimental and theoretical results. For ZrO_2:W, we checked the dopant location effect, and the obtained results showed no significant effect on the calculated values of the band gap with a maximum difference of 0.17 eV. Significant band gap tightening and optical properties of our systems indicate that these systems could be promising candidates for photoelectrochemical energy conversion (PEC) applications.

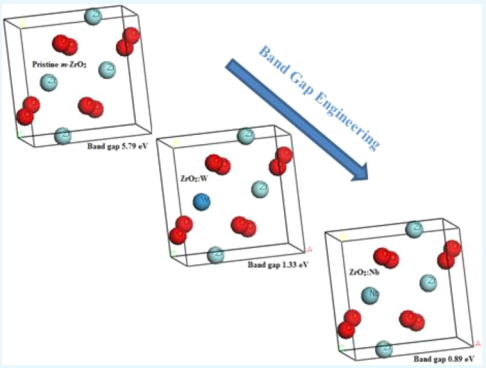

1. INTRODUCTION

Aircraft that cannot fly, factories and power stations that are closed, streets that are crowded with a huge number of vehicles that cannot be driven for even 1 km, and millions of people without jobs: this will be the situation of a world without energy. In order to avoid this scenario, scientists and researchers are working seriously toward finding new energy resources to decrease the dependence on fossil fuels.[1,2] Capturing solar energy and converting it into clean chemical energy by photoelectrochemical energy conversion (PEC) systems is considered a very promising route to overcome the shortage of nonrenewable energy globally.[3,4] In this context, researchers have made great effort to develop and discover new materials for this new technology.[5−9] Metal oxides are considered excellent candidates for this technology because of their good electrical and mechanical properties.[10,11] Furthermore, the wide band gap for metal oxides can be tailored by doping.

Zirconia (ZrO_2) is one of the most important metal oxides owing to its outstanding properties such as high dielectric constant, mechanical properties, high chemical and thermal stabilities, and wide band gaps.[12−15] ZrO_2 exists in three polymorphs, depending on the growth temperature, monoclinic (m-ZrO_2) exists at low temperatures below 1150 °C, tetragonal (t-ZrO_2) exists at intermediate temperatures between 1150 and 2370 °C, and cubic (c-ZrO_2) exists at high temperatures of more than 2370 °C. The m-ZrO_2 crystal structure is the most stable phase.[16,17]

Because of its remarkable dielectric properties, ZrO_2 is one of the most promoted candidates to replace SiO_2 in advanced metal oxide semiconductor devices.[19,20] Therefore, its structural and electronic properties have been extensively studied theoretically and experimentally.[15−25] Tolba et al.[21] studied the effect of hydrogen doping and oxygen deficiency on the electronic and optical properties of monoclinic zirconia using the density functional theory (DFT + U) approach. They concluded that defect effects mainly depend on the size and concentration. French et al.[23] studied the phase stabilization and doping effects on the electronic and optical properties of three phases of ZrO_2 using vacuum-ultraviolet and X-ray

Received: August 31, 2021
Accepted: October 14, 2021
Published: October 27, 2021

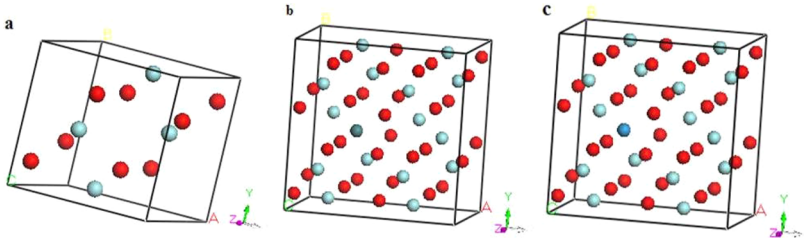

Figure 1. (a) Original m-ZrO_2 crystal, (b) and (c) super crystals 2 × 2 × 1 for ZrO_2:Nb and ZrO_2:W, respectively (oxygen atoms are in red, zirconium atoms are in baby blue, the dark gray atom in (b) is the Nb atom, and the dark blue atom in (c) is the W atom.

photoemission spectroscopies, coupled with ab initio calculations.

The band structure of *m*-ZrO_2 has been calculated using different approaches.[19,25−28] Garcia et al.[19] used the DFT-generalized gradient approximation (DFT-GGA) approach by means of the full-potential linearized augmented plane wave (FLAPW) method to determine band structure. The calculated band gap was 3.58 eV, not consistent with the experimental value 5.8 eV.[22,24] Jiang et al.[25] studied the electronic structure of crystalline ZrO_2 using the Green's function GW approximation, and the band gap was 5.34 eV. Although the result is very close to the experimental result, this approach is computationally expensive. In this regard, Li et al.[27] used the Hubbard correction (DFT + *U*) approach to include the correlation effect with low computational cost. They introduced the Coulomb interactions of 4d orbitals on the zirconium atom (U^d) and of 2p orbitals on the oxygen atom (U^p) to reproduce the experimental value.[22,24] Furthermore, applying generalized gradient approximation (GGA + *U*) and local-density approximation (LDA + *U*) approaches to wide band gap metal oxides like HfO_2 and CeO_2 was found to accurately describe the electronic structure.[28−32] Therefore, DFT calculations can be used to accurately investigate the electronic and optical structure of zirconia.

Although impurity doping has been demonstrated to be an effective way to tune photocatalytic properties, it is rarely being studied for zirconia. Xie et al.[33] investigated the effect of nitrogen doping on the electronic and magnetic properties of *m*-ZrO_2. The introduction of nitrogen in the lattice structure of zirconia improved the magnetic properties of the material with slight changes in the electronic structure. Yin et al.[34] reported the effect of nitrogen and fluorine on the carrier separation and photocatalytic activity of *m*-ZrO_2. They noticed that F doping doubled the photocatalytic activity of *m*-ZrO_2 without reducing its band gap, while F−N codoping quadrupled the photocatalytic activity. Taylor et al.[35] reported the effect of tantalum doping on the electronic and structural properties of zirconia.

In this report, we present the DFT study for the electronic, structural, and optical properties of pure and doped monoclinic zirconia (*m*-ZrO_2). Niobium and tungsten are chosen to simulate the dopant effect. The Mulliken population, band structures, density of states (DOS) dielectric functions, absorption spectra, reflective index, and reflectivity are shown in detail for the studied systems. The effect of the dopant atom location has been studied. The results presented in this report provide a clear picture of the effect of metal doping on the properties of this promising system (ZrO_2) and could be extended to other metal oxides.

2. COMPUTATIONAL METHODOLOGY

The electronic structure calculations have been performed using the spin-polarized DFT calculations based on the GGA with new parameterization that specifically targeted solids PBEsol,[9,36,37] as implemented in the CASTEP code with the plane-wave pseudopotential method.[38−40] The PBEsol parameterization is considered one of the most selective and accurate functionals to investigate the lattice constants of solids.[9] The number of plane waves induced in the basis set was determined using the kinetic energy cutoff of 750 eV. The numerical integration of the Brillouin zone was performed using the 4 × 4 × 4 Monkhorst-Pack k-point.[41] An ultrasoft pseudopotential is used to approximate the interaction between the ionic core and valence electrons. We used the Hubbard approach in order to accurately describe the energy band gap, the dopant effect, and to avoid the underestimation error of DFT.[21,27−32] The Hubbard *U* parameter was set to 8 eV for Zr 4d states and 4.35 eV for 2p states of oxygen.[27] We applied the Hubbard correction to oxygen to avoid stress over the Zr−O covalent bond that will happen if we apply the correction only on Zr 4d states.[21] During the optimization process, the parameters were set as follows: a self-consistent field tolerance of 2 × 10^{-6} eV $atom^{-1}$, maximum force of 0.05 eV $Å^{-1}$, maximum stress of 0.1 GPa, and maximum displacement of 0.002 Å. Plots of the DOSs were generated using Fermi smearing of 0.1 eV. To check the accuracy of our calculation, we first regenerate the calculation of Li et al.,[27] and we calculate the band gap without the Hubbard correction; the obtained band gap was 3.6 eV, then, we used the Hubbard correction (DFT + *U*) to regenerate the experimental band gap (5.8 eV). In our calculation, we introduced a new calculation level that we used previously.[9] We built three crystal structures: the first one for pristine ZrO_2 consists of 12 atoms, and then, we built a 2 × 2 × 1 super cell with a total number of 48 atoms to study the dopant effect. The second and third crystal structures are for the doped systems (ZrO_2:Nb) and (ZrO_2:W). They consist of 48 atoms after replacing one Zr atom with the dopant atom. To study the effect of the dopant atom location on the ZrO_2:W system, we chose four different positions (center, face, edge, and random). All the result details of the dopant location effect are available in the Supporting Information of this article (see the Supporting Information).

3. RESULTS AND DISCUSSION

3.1. Electronic and Band Structure Calculations. The crystal structure of *m*-ZrO_2 belongs to the 2/m (P 2_1/c) space group.[15,23,27] To simulate the doping effect, we have built a 2 × 2 × 1 super cell of zirconia and selected one zirconium atom in the center of the cell and replaced it once with a niobium atom (ZrO_2:Nb) and another by a tungsten atom (ZrO_2:W). The pristine single crystal consists of 12 atoms (4 Zr atoms and 8 O

https://doi.org/10.1021/acsomega.1c04756
ACS Omega 2021, 6, 30061−30068

atoms), the super cell of the niobium-doped structure consists of 48 atoms (31 Zr atoms, 12 O atoms, and 1 Nb atom) and the same for the tungsten-doped structure but with a W atom instead of a Nb atom. Figure 1 displays the investigated pristine *m*-ZrO_2 single crystal and its niobium (ZrO_2:Nb) and tungsten (ZrO_2:W) super cells. The calculated lattice parameters (a = 5.2804, b = 5.1878, and c = 5.3976 (Å) and β = 99.2336°) are in good agreement with the experimentally reported values (a = 5.17, b = 5.23, c = 5.34 (Å) and β = 99.25°)[13] and (a = 5.151, b = 5.212, c = 5.317 (Å) and β = 99.23°),[23] as well as to the average of the theoretically reported values (a = 5.22, b = 5.20, c = 5.37 (Å) and β = 99.4°).[15,21,27,34] Also, the calculated density is 5.61 gm.cc^{-3}, which is strongly consistent with the experimental value (5.18 gm.cc^{-3}).[14]

Despite many computational methods to inspect the electronic populations and charges of atomic systems, it is commonly accepted that the absolute magnitude of the atomic charges has little physical meaning because of the extreme sensitivity to the atomic basis, but the relative values are still helpful to study some physical properties of pure and doped crystal systems.[5,7,9] In this report, we analyzed Mulliken population analysis[42] to compare electronic charges and to inspect charge transfer. Table 1 displays the numerical data of Mulliken charges and band gaps of pristine and doped systems. For pristine *m*-ZrO_2, the Mulliken charges on Zr and O atoms are 1.710 and −0.855, respectively; for a niobium-doped (ZrO_2: Nb) super cell, the charges on Zr, O, and Nb are 1.714, −0.847, and 1.390 respectively, while for the tungsten-doped (ZrO_2:W) super cell, the Mulliken charges are 1.719, −0.845, and 1.220 for Zr, O, and W, respectively. These results indicate that (1) the introduction of a dopant atom slightly increases the atomic charge on both Zr and O atoms. (2) the charge transfer from metal to O decreases in the order W, Nb, and Zr, which may be due to the higher electronegativity of W (2.36) compared to Nb(1.6) and Zr(1.33),[5] (3) doping *m*-ZrO_2 and similar metal oxides with 4d and 5d metals like Nb and W may be very helpful in tuning the electronic properties of these metal oxides, which could be excellent candidates for PEC systems.

Table 1. Mulliken Charge and Bandgap of M-ZrO_2, ZrO_2:Nb, and ZrO_2:W

system	Mulliken charge				bandgap (eV)	
	Zr	O	Nb	W	direct	indirect
ZrO_2	1.710	−0.855			6.1	5.79
ZrO_2:Nb	1.714	−0.847	1.390		0.9	0.89
ZrO_2:W	1.719	−0.845		1.220	1.33	

Figure 2 shows the electronic band structures of the studied system. The pristine *m*-ZrO_2 single crystal shows an indirect band gap of 5.79 eV, which strongly correlates with the experimental value (5.8 eV)[22,24] and other theoretical reports.[16,19,21,27] The valence band maximum (VBM) is located at the G point, while the conduction band minimum (CBM) is located between A and B points; the Fermi energy (marked as the dashed line) is set to be zero energy. For doped systems, niobium-doped (ZrO_2:Nb) has an indirect band gap of 0.89 eV, the VBM is located at the Z point, and the CBM is located at the G point, while the tungsten-doped (ZrO_2:W) system shows a direct band gap of 1.33 eV, and both the VBM and CBM are located at the Q point. For both doped systems (ZrO_2:Nb and ZrO_2:W), the Fermi level shifts upward toward the conduction band, showing typical degenerate *n*-type semiconductor features,[9,43−46] which could be explained because of the higher valence of Nb and W than Zr. The band gap values of all ZrO_2:W systems with different locations of the W atom were 1.327, 1.157, 1.152, and 1.156 eV for the center, face, edge, and random positions, respectively. The difference between the obtained values is about 0.17, which

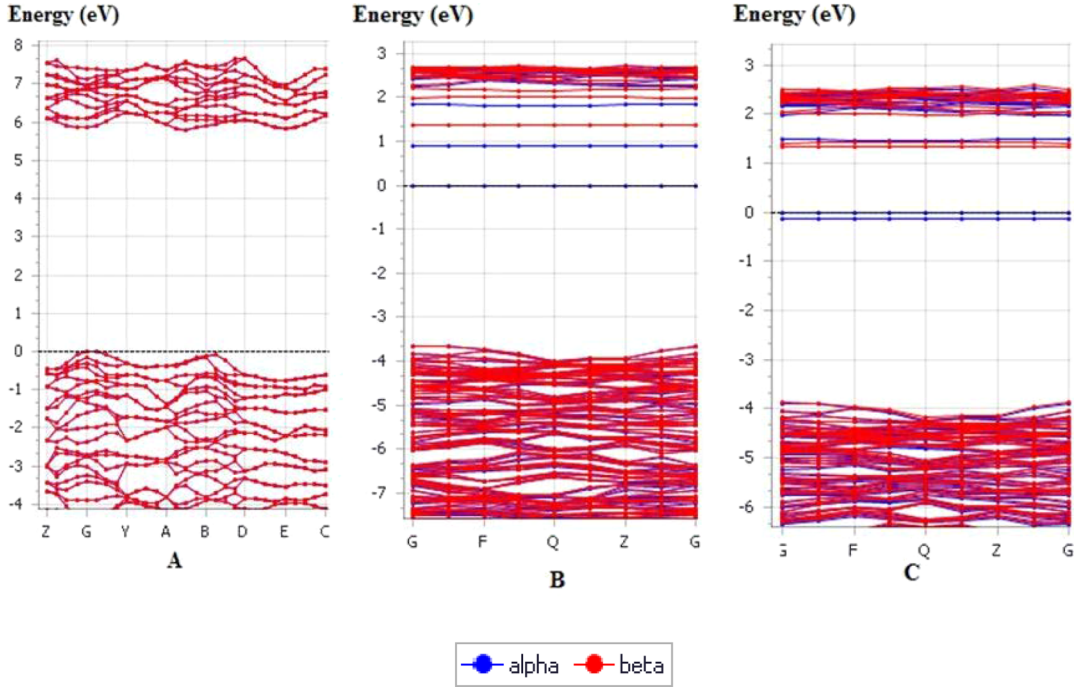

Figure 2. Band structures of (a) m-ZrO_2, (b) ZrO_2:Nb, and (c) ZrO_2:W; red curves (beta) represent contributions from spin-down eigenstates, while blue curves (alpha) represent contributions from spin-up eigenstates, and black lines (dashed lines) at 0 eV represent the Fermi level.

https://doi.org/10.1021/acsomega.1c04756
ACS Omega 2021, 6, 30061−30068

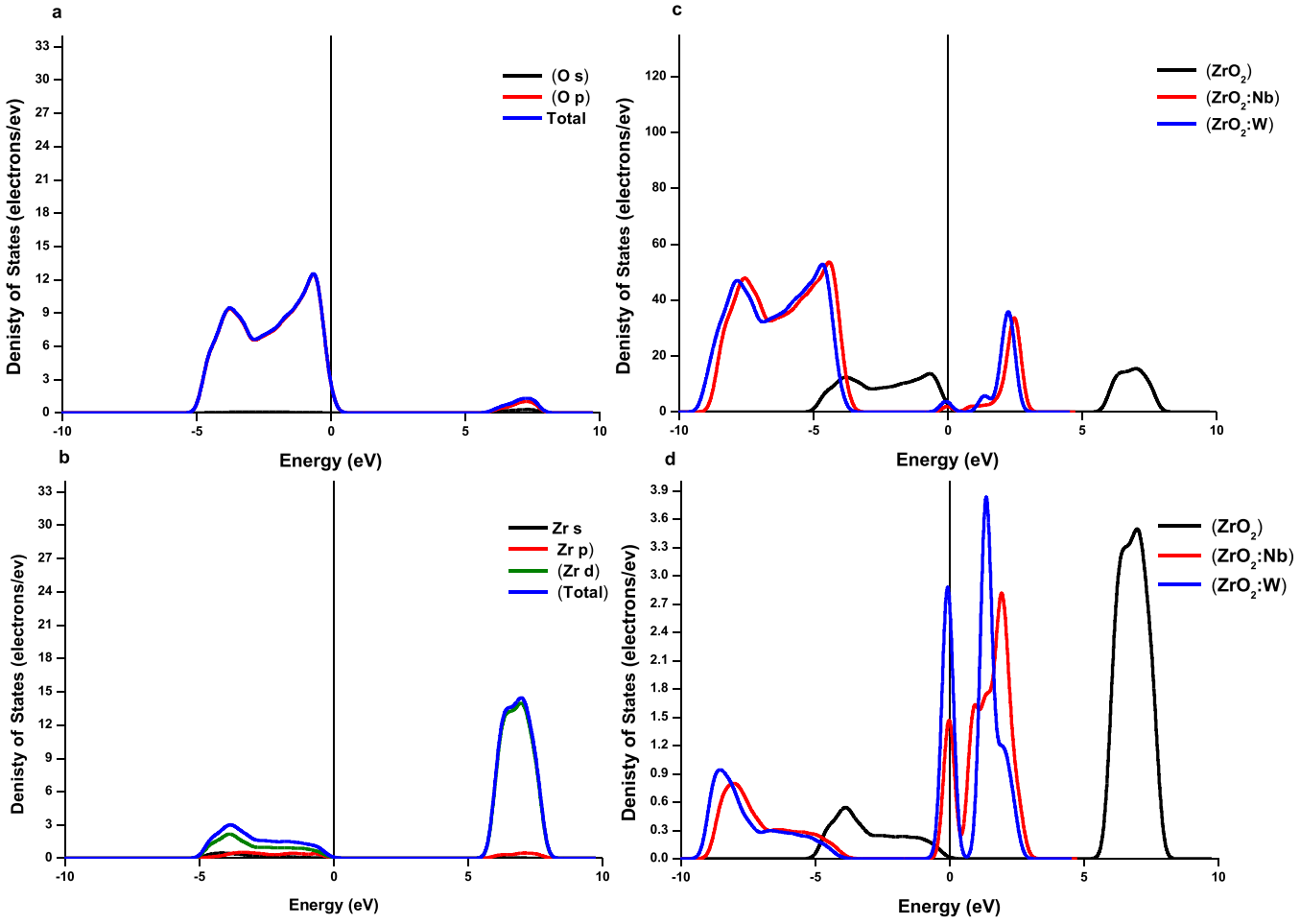

Figure 3. (a, b) PDOS of O and Zr atoms of pristine m-ZrO_2. (c) Total DOS of pristine m-ZrO_2, ZrO_2:Nb, and ZrO_2:W. (d) Partial DOS of the d orbitals of Zr, Nb, and W for *m*-ZrO_2, ZrO_2:Nb, and ZrO_2:W, respectively.

means that the doping effect does not depend on the location, which is inconsistent with some reported results.[21] It is worth mentioning that the values of the band gap of the studied systems promoted them to be promising candidates for PEC applications.

3.2. Density of States. Figure 3 depicts the total and partial DOS of pristine and doped crystals. Figure 3a,b illustrates the following: the VBM of the pristine ZrO_2 is mainly constructed by the O 2p states, while the CBM is constructed mainly by Zr 4d states. The introduction of 4d metal like (Nb) or 5d metal like W to the crystal structure of *m*-ZrO_2 is expected to modify the position of the CBM with little effect on the VBM position. Figure 3c displays the total DOS of pristine and doped crystals. Strong consistence could be noticed between the near CBM and Nb 4d and W 5d DOS in Figure 3d. However, the reduction in the band gap for the doped crystals (0.89 and 1.33 eV for ZrO_2:Nb and ZrO_2:W, respectively) could be explained because of the incorporation of 4d or 5d orbitals of dopants, which downshift the CBM with no effect on the VBM.[5] For the dopant location effect, we analyzed the DOS of all tested ZrO_2:W with different locations of the W atom (see Figure 3S in the Supporting Information), and the DOS of all tested systems is almost the same, reflecting the nonsignificant effect of the dopant location, consistent with the very close values of the band gap for different ZrO_2:W crystals with different locations of W atoms.

3.3. Optical Properties. In order to investigate in-depth and further understand the investigated systems, the optical properties have been studied to clarify the doping effect on *m*-ZrO_2. We used the dielectric function $[\varepsilon(W) = \varepsilon_1(W) + i\varepsilon_2(W)]$ to investigate the optical properties of pristine and doped crystals. The imaginary part $\varepsilon_2(W)$ could be calculated using the momentum matrix element and is given by the following expression:[47−49]

$$\varepsilon_2 = \frac{2\pi e^2}{\Omega \varepsilon_0} \sum_{k,v,c} |\langle \varphi_k^c | \hat{u} r | \varphi_k^v \rangle|^2 \delta(E_k^v - E) \quad (1)$$

where e is the electronic charge, Ω is the volume of the unit cell, φ is the light frequency, $\hat{u}$ is the vector defining the polarization of the incident field, and φ_k^c and φ_k^v are the wave functions of conduction and valence bands at k, respectively. Using the Kramers−Kronig relation,[5,7,9,47,48] one can derive the real part $\varepsilon_1(W)$. Other optical properties such as the absorption spectrum $\alpha(W)$, the imaginary part of the refractive index $n(W)$, and the imaginary part of the refractive index $k(W)$ can be derived from $\varepsilon_1(W)$ and $\varepsilon_2(W)$, as given by eqs 2−5.

$$\alpha(W) = \sqrt{2W}\,[\sqrt{\varepsilon_1^2(W) + \varepsilon_2^2(W)} - \varepsilon_1(W)]^{1/2} \quad (2)$$

https://doi.org/10.1021/acsomega.1c04756
ACS Omega 2021, 6, 30061−30068

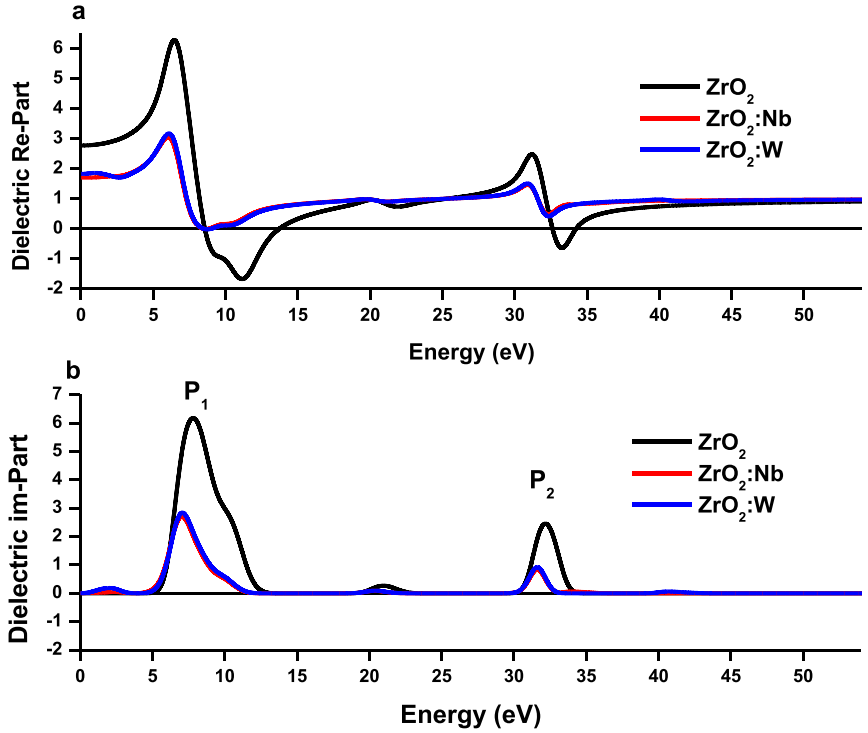

Figure 4. Dielectric constant of the studied systems (a) real part and (b) imaginary part.

$$R(\mathrm{W}) = \left| \frac{\sqrt{\varepsilon_1^2(\mathrm{W}) + j\varepsilon_2^2(\mathrm{W})} - 1}{\sqrt{\varepsilon_1^2(\mathrm{W}) + j\varepsilon_2^2(\mathrm{W})} + 1} \right|^2 \quad (3)$$

$$n(\mathrm{W}) = \left[\sqrt{\varepsilon_1^2(\mathrm{W}) + j\varepsilon_2^2(\mathrm{W})} + \varepsilon_1(\mathrm{W})\right]^{1/2} \Big/ \sqrt{2} \quad (4)$$

$$k(\mathrm{W}) = \left[\sqrt{\varepsilon_1^2(\mathrm{W}) + j\varepsilon_2^2(\mathrm{W})} - \varepsilon_1(\mathrm{W})\right]^{1/2} \Big/ \sqrt{2} \quad (5)$$

Figure 4 shows the real part ε_1 (a) and imaginary part ε_2 (b) of pristine and doped crystals. The calculated dielectric constant is 2.77, which is lower than the experimental value (4.1),[49] and this is because using values of U higher than 4 leads to an underestimation of the dielectric constant when compared to the experimental values.[15] The introduction of niobium (Nb) and tungsten (W) in the crystal structure of *m*-ZrO_2 decreased the dielectric constant in the following order: 2.77, 1.83, and 1.71 for *m*-ZrO_2, ZrO_2:W, and ZrO_2:Nb, respectively (Figure 4a). Despite the higher dielectric constant of pristine (2.77) than doped crystals (1.83, 1.71), the electronic contribution of the doped systems from 10 to 45 eV is higher than that of pristine systems. Also, the peaks below zero reflect the near-metallic behavior of the studied systems. From Figure 4a, it is easy to notice the disappearance of the negative value of the real part of the dielectric constant, which could be explained as a direct result of the introduction of 4d and 5d metals (Nb and W) in the crystal structure of *m*-ZrO_2.

We can investigate the electronic transition from the occupied orbitals to the unoccupied orbitals from the main peaks of the imaginary part. For pristine ZrO_2, we have two main peaks (P1, P2) at 10 and 35 eV, respectively, and a minor peak at 22 eV (Figure 4b), and these peaks correspond to the electronic transition from O 2p of the valence band to Zr 4d of the conduction band, coinciding with the previous findings.[19,21,27] At zero electron voltage, the dielectric constant of the doped crystals (ZrO_2:Nb, ZrO_2:W) is higher than that of pure ZrO_2, reflecting the better light absorption characteristics because of good interactions between the electrons and photons.

The absorption spectra of the studied systems are illustrated in Figure 5a. The spectra indicate the fraction of energy lost by the electromagnetic wave when it passes through the material.[5,7] The spectral result of pristine ZrO_2 is in good consistency with the result of Yin et al.,[34] in which the absorption edge is located at 220 nm, and the absorbance is recorded in the wavelength range of 200−650 nm. For the doped systems, the incorporation of Nb and W increased the optical absorption in the visible and near-infrared regions that matches with the higher dielectric of the imaginary part at zero voltage because of higher interactions between electrons and photons.

The reflectivity $R(\mathrm{W})$ of the studied systems is shown in Figure 5b. The spectrum of pristine ZrO_2 consists of two main peaks, and the maximum reflectivity is recorded at 15 eV, matching with the previous theoretical[19] and experimental reports.[23,49] For the doped systems, they reached the maximum reflectivity at 7 eV. The higher reflectivity of studied systems indicates the potential of the use of these systems as PEC devices.

Also, the real $n(\mathrm{W})$ and imaginary $k(\mathrm{W})$ parts of the refractive index are calculated, as shown in Figure 5c,d. The static refractive index $n(\mathrm{W} = 0)$ of the pristine crystal was found to be ≈ 1.7, which is in good agreement with the result of Garcia et al. (2.3).[19] where the index values of doped crystals ZrO_2:Nb and ZrO_2:W were 1.3 and 1.35, respectively. The imaginary part consists of two main peaks for three crystals, but ZrO_2:W has an additional peak at 3 eV.

https://doi.org/10.1021/acsomega.1c04756
ACS Omega 2021, 6, 30061−30068

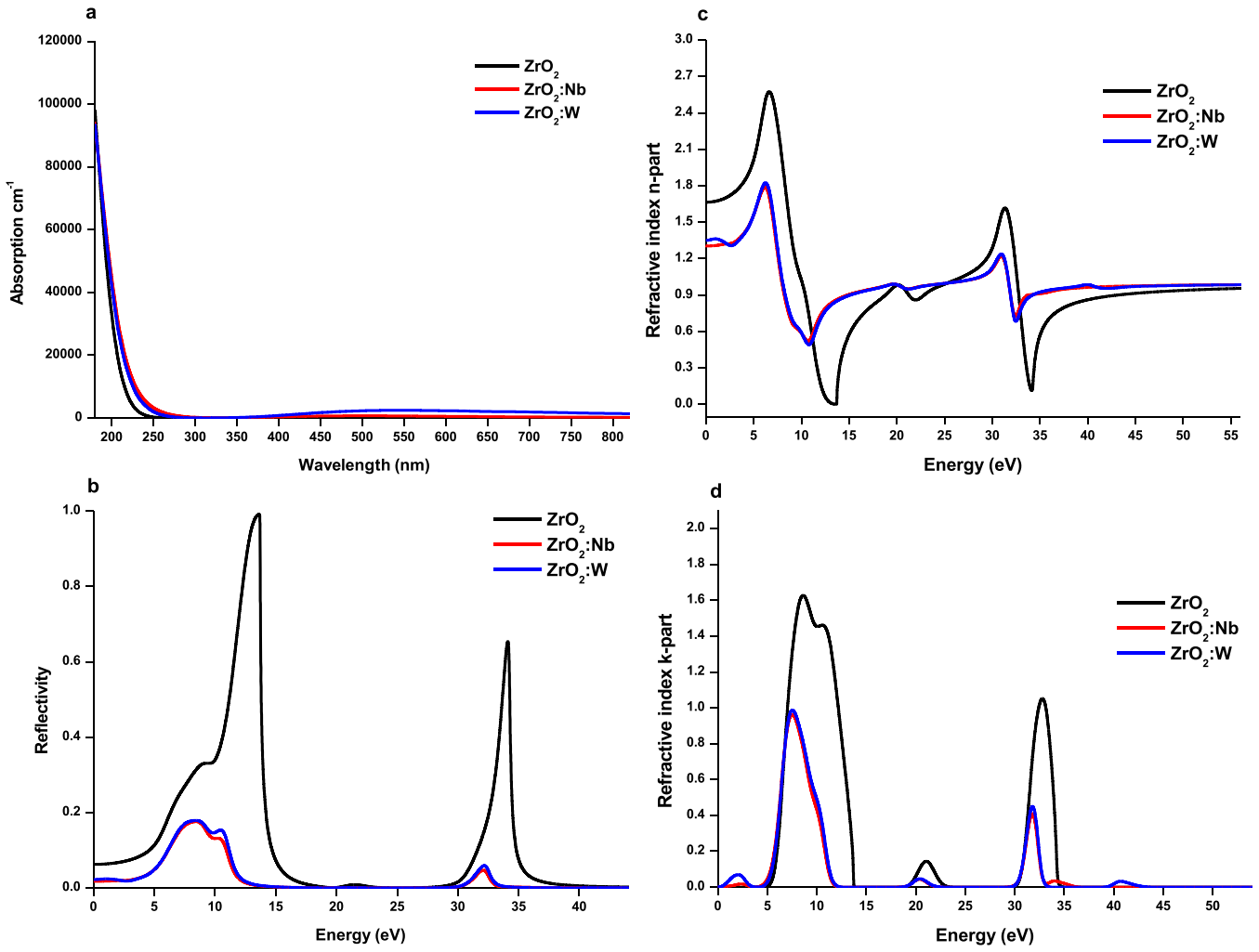

Figure 5. Optical properties of the studied systems (a) absorption spectrum, (b) reflectivity spectrum, (c) and (d) real and imaginary parts of the refractive index.

4. SUMMARY AND CONCLUSIONS

In summary, first-principles calculations using the Hubbard approach (DFT + *U*) with the PBEsol correlation were carried out to study the effects of Nb and W doping on the electronic and optical properties of pristine ZrO_2. We applied the optimal values of U^d (8 eV) and U^p (4.35 eV) in order to reproduce the experimental band gap. For pristine ZrO_2, the calculations indicated an indirect band gap of 5.79, which is in good agreement with the experimental and direct band gap of 6.1 eV. The introduction of Nb and W in the crystal structure of pristine ZrO_2 led to the displacement of the band gap edges and reallocation of the Fermi level. The VBM shifted upward, resulting in band gap tightening from 5.79 to 0.89 for ZrO_2:Nb and to 1.33 eV for ZrO_2:W. The total DOS and PDOS calculations indicated that the VBM of pristine ZrO_2 is mainly constructed by O 2p states, while the CBM is constructed mainly by Zr 4d states. However, the doped crystals of the CBM are mainly constructed by 4d and 5d states of Nb and W, respectively. Furthermore, the optical absorption of the doped crystals extended into the visible and near-infrared regions, which was confirmed by a higher dielectric of the imaginary part at zero voltage. For pristine ZrO_2, the results obtained for the imaginary and real parts of the dielectric function, the refractive index, and the reflectivity show good agreement with the available experimental and theoretical results. For the dopant location effect, the band structure and DOS of different ZrO_2:W systems with different locations of W atoms reflect nonsignificant. The promising results we mentioned above highly promote the studied crystals to be excellent candidates for solar energy conversion devices.

FINANCIAL SUPPORT

This research did not receive any specific grant from funding agencies in the public, commercial, or not-for-profit sectors.

ASSOCIATED CONTENT

Supporting Information

The Supporting Information is available free of charge at https://pubs.acs.org/doi/10.1021/acsomega.1c04756.

Crystal structures, band structures, and DOS of ZrO_2:W with different locations of W atoms is available (PDF)

AUTHOR INFORMATION

Corresponding Author

El-Sayed R. Khattab − *Department of Chemistry, Faculty of Science, Ain-Shams University, Cairo 11566, Egypt;* orcid.org/0000-0002-0302-1101; Email: sayedkhatab2010@yahoo.com

https://doi.org/10.1021/acsomega.1c04756
ACS Omega 2021, 6, 30061−30068

Authors

Sayed S. Abd El Rehim − *Department of Chemistry, Faculty of Science, Ain-Shams University, Cairo 11566, Egypt*

Walid M. I. Hassan − *Department of Chemistry, Faculty of Science, Cairo University, Giza 12613, Egypt*

Tamer S. El-Shazly − *Department of Chemistry, Faculty of Science, Ain-Shams University, Cairo 11566, Egypt*

Complete contact information is available at: https://pubs.acs.org/10.1021/acsomega.1c04756

Notes

The authors declare no competing financial interest.

■ ACKNOWLEDGMENTS

We would like to thank King Abdulaziz University in Saudi Arabia for the technical support of this research.

■ REFERENCES

(1) Chen, X.; Shen, S.; Guo, L.; Mao, S. S. Semiconductor-based photocatalytic hydrogen generation. *Chem. Rev.* **2010**, *110*, 6503−6570.

(2) Wang, W.; Tadé, M. O.; Shao, Z. Research progress of perovskite materials in photocatalysis- and photovolatics-related energy conversion and environmental treatment. *Chem. Soc. Rev.* **2015**, *44*, 5371−5408.

(3) Xiang, Q.; Cheng, B.; Yu, J. Graphene-based photocatalysts for solar-fuel generation. *Angew. Chem., Int. Ed.* **2015**, *54*, 11350−11366.

(4) Nashed, R.; Szymanski, P.; el-Sayed, M. A.; Allam, N. K. Self-Assembled nanostructured photoanodes with staggered bandgap for efficient solar energy conversion. *ACS Nano* **2014**, *8*, 4915−4923.

(5) el-Shazly, T. S.; Hassan, W. M. I.; Abdel Rahim, S. T.; Allam, N. K. Unravelling the interplay of dopant concentration and band structure engineering of monoclinic niobium pentoxide: A model photoanode for water splitting. *Int. J. Hydrogen Energy* **2015**, *40*, 13867−13875.

(6) Amer, W.; el-Sayed, M. A.; Allam, N. K. Tuning the photoactivity of zirconia nanotubes-based photoanodes via ultra-thin layers of ZrN: an effective approach towards visible light-water splitting. *J. Phys. Chem. C.* **2016**, *120*, 7025−7032.

(7) el-Shazly, T. S.; Hassan, W. M.; Abd el Rehim, S. S.; Allam, N. K. Optical and electronic properties of niobium oxynitrides with various N/O ratios: insights from first-principles calculations. *J. Photon. Energy* **2018**, *8*, 1.

(8) Yu, H. X.; Mu, H. M.; Zhu, D. R.; Zhang, Y.; Wang, X. C.; Xiao-An Zhang, S. DFT study on the oxygen titanium porphyrin as sustainable cyclic catalyst for water splitting. *Int. J. Hydrogen Energy* **2019**, *44*, 19920−19928.

(9) el-Shazly, T. S.; Hassan, W. M. I.; Rehim, S. S. A.; Allam, N. K. DFT insights into the electronic and optical properties of fluorinedoped monoclinic niobium pentoxide (B-Nb2O5:F). *Appl. Phys. A: Mater. Sci. Process.* **2016**, *122*, 859−865.

(10) Awad, N. K.; Ashour, E. A.; Allam, N. K. Recent advances in the use of metal oxide based photocathodes for solar fuel production. *J. Renew. Sustain. Energy* **2014**, *6*, No. 022702.

(11) Zahedi, E.; Hojamberdiev, M.; Bekheet, M. F. Effective masses, electronic and optical properties of (111)-layered B-site deficient hexagonal perovskite $Ba_5M_4O_{15}$ (M 1/4 Ta, Nb): a DFT study using HSE06. *RSC Adv.* **2016**, *6*, 61150−61161.

(12) Zhu, W.; Wang, R.; Shu, G.; Wu, P.; Xiao, H. First-principles study of the structure, mechanical properties, and phase stability of crystalline zirconia under high pressure. *Struct. Chem.* **2012**, *23*, 601−611.

(13) Lowther, J. E.; Dewhurst, J. K.; Leger, J. M.; Haines, J. Relative stability of ZrO_2 and HfO_2 structural phases. *Phys. Rev. B* **1999**, *60*, 14485−14488.

(14) Martin, P. J.; Netterfield, R. P.; Sainty, W. G. Modification of the optical and structural properties of dielectric Zr02 films by ion-assisted deposition. *J. Appl. Phys.* **1984**, *55*, 235−241.

(15) Delarmelina, M.; Quesne, M. G.; Catlow, C. R. A. Modelling the bulk properties of ambient pressure polymorphs of zirconia†. *Phys. Chem. Chem. Phys.* **2020**, *22*, 6660−6676.

(16) Zhao, X. S.; Shang, S. L.; Liu, Z. K.; Shen, J. Y. Elastic properties of cubic, tetragonal and monoclinic ZrO_2 from first-principles calculations. *J. Nucl. Mater.* **2011**, *415*, 13−17.

(17) Dash, L.; Vast, N.; Baranek, P.; Cheynet, M. C.; Reining, L. Electronic structure and electron energy-loss spectroscopy of ZrO_2 zirconia. *Phys. Rev. B* **2004**, *70*, 245116−245133.

(18) Lopes, J. E. M.; Oliveira, M. M.; Costa, M. . G. S.; de Figueredo, G. P.; Vasconcelos, J. S.; Rangel, J. H. G. Chemical synthesis and characterization of Nb−ZrO_2. *Ceram. Int.* **2016**, *42*, 861−873.

(19) Garcia, J.; Scolfaro, L.; Lino, A.; Freire, V.; Farias, G.; Silva, C.; Alves, H. W. L.; Rodrigues, S.; da Silva, E. F., Jr. Structural, electronic, and optical properties of ZrO_2 from ab initio calculations. *J. Appl. Phys.* **2006**, *100*, 104103−104112.

(20) Wang, Y.; Zhang, Y.; Lu, H.; Chen, Y.; Liu, Z.; Su, S.; Xue, Y.; Yao, J.; Zeng, H. Novel N-doped ZrO_2 with enhanced visible-light photocatalytic activity for hydrogen production and degradation of organic dyes. *RSC Adv.* **2018**, *8*, 6752−6758.

(21) Tolba, S. A.; Allam, N. K. Computational design of novel Hydrogen-Doped, Oxygen-Deficient monoclinic zirconia with excellent optical absorption and electronic properties. *Sci. Rep.* **2019**, *9*, 10159.

(22) Houssa, M.; Afanas'ev, V. V.; Stesmans, A.; Heyns, M. M. Variation in the fixed charge density of SiOx / ZrO2 gate dielectric stacks during postdeposition oxidation. *Appl. Phys. Lett.* **2000**, *77*, 1885−1887.

(23) French, R. H.; Glass, S. J.; Ohuchi, F. S.; Xu, Y.-N.; Ching, W. Y. Experimental and theoretical determination of the electronic structure and optical properties of three phases of ZrO_2. *Phys. Rev. B* **1994**, *49*, 5133−5142.

(24) Zhao, X.; Vanderbilt, D. Phonons and lattice dielectric properties of zirconia. *Phys. Rev. B* **2002**, *65*, No. 075105.

(25) Jiang, H.; Gomez-Abal, R. I.; Rinke, P.; Scheffler, M. Electronic band structure of zirconia and hafnia polymorphs from the GW perspective. *Phys. Rev. B* **2010**, *81*, No. 085119.

(26) Qunbo, F.; Fuchi, W.; Huiling, Z.; Feng, Z. Study of ZrO_2 phase structure and electronic properties. *Mol. Simul.* **2008**, *34*, 1099−1103.

(27) Li, J.; Meng, S.; Niu, J.; Lu, H. Electronic structures and optical properties of monoclinic ZrO_2 studied by first-principles local density approximation + U approach. *J. Adv. Ceram.* **2017**, *6*, 43−49.

(28) Plata, J. J.; Márquez, A. M.; Sanz, J. F. Communication: Improving the density functional theory+U description of CeO_2 by including the contribution of the O 2p electrons. *J. Chem. Phys.* **2012**, *136*, No. 041101.

(29) Li, J.; Meng, S.; Li, L.; Lu, H.; Tohyama, T. First-principles generalized gradient approximation (GGA)+U^d+U^p studies of electronic structures and optical properties in cubic HfO_2. *Comput. Mater. Sci.* **2014**, *81*, 397−401.

(30) Li, J.; Han, J.; Meng, S.; Lu, H.; Tohyama, T. Optical properties of monoclinic HfO2 studied by first-principles local density approximation + U approach. *Appl. Phys. Lett.* **2013**, *103*, No. 071916.

(31) Loschen, C.; Carrasco, J.; Neyman, K. M.; Illas, F. First-principles LDA+U and GGA+U study of cerium oxides: Dependence on the effective U parameter. *Phys. Rev. B* **2007**, *75*, No. 035115.

(32) Zhang, Y.; Jiang, H. Intra- and Interatomic Spin Interactions by the Density Functional Theory plus U Approach: A Critical Assessment. *J. Chem. Theory Comput.* **2011**, *7*, 2795−2803.

(33) Xie, Y.; Zhou, A. N.; Zhang, Y. T.; Huo, Y. P.; Wang, S. F.; Zhang, J. M. First principles study of structural, magnetic and electronic properties of N-doped monoclinic ZrO_2. *J. Magn. Magn. Mater.* **2015**, *387*, 58−61.

(34) Yin, S.; Chen, J.; Wu, Y.; Chen, Z.; Yuan, T.; Liu, Q.; Wang, Y.; Hou, H. Mechanisms of impurity-enhanced spatial carrier separation and photocatalytic activity of F−N codoped m-ZrO2 nanocrystals. *J. Phys. Chem. Solids* **2020**, *140*, No. 109363.
(35) Taylor, M.; Alonso, R.; Errico, L.; López-García, A.; de la Presa, P.; Svane, A.; Christensen, N. Structural, electronic, and hyperfine properties of pure and Ta-doped *m*-ZrO_2. *Phys. Rev. B* **2012**, *85*, No. 155202.
(36) Pérez-Walton, S.; Valencia-Balvín, C.; Dalpian, G. M.; Osorio-Guillén, J. M. Electronic, dielectric, and optical properties of the B phase of niobium pentoxide and tantalum pentoxide by first principles calculations. *Phys. Status Solidi B* **2013**, *250*, 1644−1650.
(37) Perdew, J. P.; Ruzsinszky, A.; Csonka, G. I.; Vydrov, O. A.; Scuseria, G. E.; Constantin, L. A.; Zhou, X.; Burke, K. Restoring the density-gradient expansion for exchange in solids and surfaces. *Phys. Rev. Lett.* **2008**, *100*, No. 136406.
(38) Segall, M. D.; Lindan, P. J. D.; Probert, M. J.; Pickard, C. J.; Hasnip, P. J.; Clark, S. J.; Payne, M. C. First-principles simulation: ideas, illustrations and the CASTEP code. *J. Phys.: Condens. Matter* **2002**, *14*, 2717−2744.
(39) Payne, M. C.; Teter, M. P.; Allan, D. C.; Arias, T. A.; Joannopoulos, J. D. Iterative minimization techniques for ab initio total-energy calculations: molecular dynamics and conjugate gradients. *Rev. Mod. Phys.* **1992**, *64*, 1045−1097.
(40) David, V. Soft self-consistent pseudopotentials in a generalized eigenvalue formalism. *Phys. Rev. B* **1990**, *41*, 7892−7895.
(41) Monkhorst, H. J.; Pack, J. D. Special points for Brillouin-zone integrations. *Phys. Rev. B* **1976**, *13*, 5188−5192.
(42) Mulliken, R. Electronic population analysis on LCAOMO molecular wave functions. I. *J. Chem. Phys.* **1955**, *23*, 1833−1840.
(43) Jiang-Ni, Y.; Zhi-Yong, Z. Electronic structure and optical properties of Nb-doped Sr2TiO4 by density function theory calculation. *Chin. Phys. B* **2009**, *18*, 2945−2952.
(44) Liu, X. D.; Jiang, E. Y.; Li, Z. Q.; Song, Q. G. Electronic structure and optical properties of Nb-doped anatase TiO_2. *Appl. Phys. Lett.* **2008**, *92*, 252104.
(45) Huang, B.; Hart, J. N. DFT study of various tungstates for photocatalytic water splitting. *Phys. Chem. Chem. Phys.* **2020**, *22*, 1727−1737.
(46) Wu, T.; Deng, Q.; Hansen, H. A.; Vegge, T. Mechanism of Water Splitting on Gadolinium-Doped CeO_2 (111): A DFT + *U* Study. *J. Phys. Chem. C* **2019**, *123*, 5507−5517.
(47) Saha, S.; Sinha, T. P.; Mookerjee, A. Electronic structure, chemical bonding, and optical properties of paraelectric BaTiO3. *Phys. Rev. B* **2000**, *62*, 8828−8834.
(48) al-Aqtash, N.; Apostol, F.; Mei, W. N.; Sabirianov, R. F. Electronic and optical properties of TaO1-xN1?x based alloys. *J. Solid State Chem.* **2013**, *198*, 337−343.
(49) Camagni, P.; Samoggia, G.; Sangaletti, L.; Parmigiani, F.; Zema, N. X-ray-photoemission spectroscopy and optical reflectivity of yttrium-stabilized zirconia. *Phys. Rev. B* **1994**, *50*, 4292−4296.

https://doi.org/10.1021/acsomega.1c04756
ACS Omega 2021, 6, 30061−30068